Available online at www.sciencedirect.com
ScienceDirect
Dyes and Pigments 74 (2007) 396–403
DYES and PIGMENTS
www.elsevier.com/locate/dyepig

Amphiphilic azo-dyes (**RED-PEGM**). Part 2: Charge transfer complexes, preparation of Langmuir–Blodgett films and optical properties

Ernesto Rivera [a,*], Maria del Pilar Carreón-Castro [b], Lorena Rodríguez [a], Gerardo Cedillo [a], Serguei Fomine [a], Omar G. Morales-Saavedra [c]

[a] *Instituto de Investigaciones en Materiales UNAM, Circuito Exterior Ciudad Universitaria, C.P. 04510, México D.F., Mexico*
[b] *Instituto de Ciencias Nucleares UNAM, Circuito Exterior Ciudad Universitaria, C.P. 04510, México D.F., Mexico*
[c] *Centro de Ciencias Aplicadas y Desarrollo Tecnológico UNAM, Circuito Exterior Ciudad Universitaria, C.P. 04510, México D.F., Mexico*

Received 17 February 2006; accepted 23 February 2006
Available online 21 April 2006

Abstract

Optical properties of three amphiphilic azo-dyes bearing end-capped oligo(ethylene glycol) segments: *N*-methyl-*N*-{4-[(*E*)-(4-nitrophenyl)-diazenyl] phenyl}-*N*-(3, 6, 9-trioxadecas-1-yl)amine (**RED-PEGM-3**), *N*-methyl-*N*-{4-[(*E*)-(4-nitrophenyl)diazenyl] phenyl}-*N*-(3, 6, 9, 12, 15, 18, 21, 24-octaoxapentaeicos-1-yl)amine (**RED-PEGM-8**) and *N*-methyl-*N*-{4-[(*E*)-(4-nitrophenyl)diazenyl] phenyl}-*N*-(3, 6, 9, 12, 15, 18, 21, 24, 27, 30)-decaoxauntricontas-1-yl)amine (**RED-PEGM-10**) were studied in Z-type LB films by absorption spectroscopy. **RED-PEGM-8** and **RED-PEGM-10** formed intramolecular charge transfer complexes in aqueous solution due to coiling of the end-capped poly(ethylene glycol) side-chain around the azobenzene groups. This was detected by ^{1}H NMR, 2D NOESY spectroscopy and the optimised geometries of the complexes were estimated by DFT calculations. The formation and optical properties of CT complexes are discussed with respect to the poly(ethylene glycol) segments length. Z-type Langmuir–Blodgett (LB) films of **RED-PEGM-8** exhibited $\chi^{(2)}$ non-linear optical properties (NLO) like second harmonic generation (SHG) depending on the number of deposited layers. The $\chi^{(2)}_{31}$ and $\chi^{(2)}_{33}$ NLO-coefficients were evaluated to be approximately 2.7 and 12.5 pm V^{-1}, respectively for a single **RED-PEGM-8** layer sample.

Keywords: Charge transfer; Azobenzene; Poly(ethylene glycol); Langmuir–Blodgett films; Optical properties

1. Introduction

Due to its water solubility, poly(ethylene glycol) (PEG) is an attractive polymer for generating multicomponent structures and for solvent-selective combination [1]. It has often been used in the synthesis of ion conducting materials [2] because of its ability to complex cations and form charge transfer (CT) complexes [3]. Recently, Cojocariu and Natansohn showed how an end-capped oligo(ethylene glycol) methyl ether 3,5-dinitrobenzoate (DNB) formed an intramolecular CT complex in water due to the coiling of the highly hydrophilic poly(ethylene glycol) methyl ether (PEGM) chain around the hydrophobic DNB unit [4].

On the other hand, azobenzene dyes have been widely studied by many research groups. Rau classified azobenzenes into three main groups based on their photochemical behaviour [5]. Unsubstituted photochromic azobenzene makes up the first group, known simply as ''azobenzenes''. The thermally stable *trans*-form exhibits a strong π–π* transition at 313 nm and a weak n–π* transition at 436 nm, whereas the *cis*-form undergoes similar transitions but with a more intense n–π* band. In addition, ''azobenzenes'' have a relatively poor π–π* and n–π* overlaps. The second group, known as ''aminoazobenzenes'' typically include azobenzenes that are substituted by an electron-donor group and are characterized by overlapping π–π* and n–π* bands. Finally, azobenzenes bearing

* Corresponding author. Fax: +52 55 56 16 12 01.
E-mail address: riverage@zinalco.iimatercu.unam.mx (E. Rivera).

0143-7208/$ - see front matter © 2006 Elsevier Ltd. All rights reserved.
doi:10.1016/j.dyepig.2006.02.023

both electron-donor and electron-acceptor groups belong to the third group, ''pseudostilbenes'', where the π–π* and n–π* bands are practically superimposed but are actually inverted on the energy scale with respect to the ''azobenzene'' bands [5].

Donor–acceptor substituted azobenzene units incorporated into a polymer main-chain or side-chain provide very versatile materials from an applications point of view. In particular, pseudostilbene azobenzenes undergo rapid *trans–cis–trans* photoisomerization cycles when irradiated with absorbing laser light. The use of polarized radiation allows for the selective activation of pseudostilbenes with polarization axis parallelizing the absorbing radiation [6–12].

Azobenzene molecules are also known to undergo chromic changes through aggregation in various media including solution, spin-cast films and Langmuir–Blodgett layers. Aggregation and chromic changes within these systems are described by in-line or J-type aggregation and side-on or H-type aggregation [13]. Azobenzene and poly(ethylene glycol) have been incorporated into more sophisticated systems such as copolymers [14,15], nanomaterials [16,17], cellulose derivatives [18,19] and cyclodextrin polymers [20,21], in some cases forming supramolecular complexes with interesting properties [22].

Previously, we reported the synthesis and full characterization of *N*-methyl-*N*-{4-[(*E*)-(4-nitrophenyl)diazenyl] phenyl}-*N*-(3, 6, 9, 12, 15, 18, 21, 24-octaoxapentacos-1-yl)amine (**RED-PEGM-8**) [23]. This dye readily forms H-aggregates in concentrated aqueous solutions and cast films. The presence of J-aggregates was not observed for this compound, but the presence of head to head J-aggregates was detected in Y-type LB films [24]. In the present work, we studied the formation of intramolecular charge transfer complexes of **RED-PEGM-8** and two related azo-dyes: *N*-methyl-*N*-{4-[(*E*)-(4-nitrophenyl)diazenyl] phenyl}-*N*-(3, 6, 9-trioxadecas-1-yl)amine (**RED-PEGM-3**) and *N*-methyl-*N*-{4-[(*E*)-(4-nitrophenyl)diazenyl] phenyl}-*N*-(3, 6, 9, 12, 15, 18, 21, 24, 27, 30)-decaoxauntricontas-1-yl)amine (**RED-PEGM-10**) in dilute solutions (molecular structures are shown in Fig. 1). On the other hand, Z-type LB films of these azo-dyes were prepared and the nonlinear optical properties of **RED-PEGM-8** were studied as function of the number of layers.

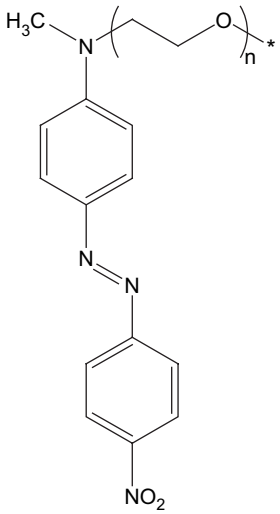

n = 3, RED-PEGM-3
n = 8, RED-PEGM-8
n = 10, RED-PEGM-10

Fig. 1. Structure of the amphiphilic azo-dyes (**RED-PEGM**).

2. Experimental section

N-Methyl-*N*-{4-[(*E*)-(4-nitrophenyl)diazenyl] phenyl}-*N*-(3, 6, 9-trioxadecas-1-yl)amine (**RED-PEGM-3**), *N*-methyl-*N*-{4-[(*E*)-(4-nitrophenyl)diazenyl] phenyl}-*N*-(3, 6, 9, 12, 15, 18, 21, 24-octaoxapentaeicos-1-yl)amine (**RED-PEGM-8**) and *N*-methyl-*N*-{4-[(*E*)-(4-nitrophenyl)diazenyl] phenyl}-*N*-(3, 6, 9, 12, 15, 18, 21, 24, 27, 30)-decaoxauntricontas-1-yl)-amine (**RED-PEGM-10**) were synthesized according to the method previously reported by us [23].

The absorption spectra of Z-type LB films of the azo-dyes were recorded on a Varian Cary 1 Bio UV–vis (model 8452A) spectrophotometer at room temperature. ^{1}H NMR spectra were recorded in D_2O at room temperature on a Bruker Avance 400 MHz spectrometer. Dipole moments (μ) and optimised geometries of all these dyes were estimated by semi-empirical calculations using AM1 and PM3 methods and by DFT calculations using B3LYP/aug-cc-PVTZ(-f)//BHandH/G-31G* level of theory [25].

Langmuir–Blodgett membranes were prepared using an LB trough NIMA 622D2 (NIMA Technology Coventry, UK) equipped with a Wilhelmy plate surface pressure sensor. Spreading solutions were prepared by dissolving the azo-dyes in chloroform (HPLC grade) at a concentration in the range of 0.8–1.5 mg/ml. The monolayer was formed by spreading 100–150 μl of the solution on the water subphase, which had been purified by a Milli-Q system (Millipore), $\rho = 18.2$ MΩ cm). The films were compressed after 15–20 min of equilibration with a constant barrier speed of 5 cm^2/min. The isotherms were recorded at 22 ± 1 °C. Multilayers were formed by depositing the monolayers at a target pressure of 25 mN/m and a dipper speed of 5–10 mm/min. A transfer ratio between 0.8 and 1.0 was observed.

Quartz and glass were used as substrates in this work and were washed with chloroform, acetone and ethanol successively in an ultrasonic bath before use. Clean substrates (quartz and glass) were hydrophobized by treating them with ferric stearate prior to deposition. Z-type LB-multilayers were prepared with the **RED-PEGM** dyes.

Brewster angle microscopy (BAM) images were taken with a BAM2plus set-up from Nanofilm Technologies, GmbH, using an argon laser illusion and a CCD camera for recording. The field used was 620 μm in width and 500 μm in height. Atomic force microscopy (AFM) of the LB films was carried out using a Nanoscope IIIa from Digital Instruments, Inc., and the images were recorded in contact mode at room temperature. The scan speed was 1.5 Hz and low scanning forces (0.3 N/m) were employed to avoid any surface damage.

2.1. Second harmonic generation – measurements

Mono- and multilayer samples of Z-type LB films of **RED-PEGM-8** deposited on glass substrates were studied as active media for SHG. The SHG-technique is shown schematically in Fig. 2. A commercial diode pumped passive Q-switched Cr:Nd:YAG Laser system, operating at $\lambda_\omega = 1064$ nm, with a repetition rate of 25 KHz and a pulse duration of $\tau = 5$ ns (Smart Laser Systems, SMS-Berlin) was implemented to provide the fundamental wave. Typical pulse powers of 120 μJ were integrated with an optical chopper (50 Hz) and the intensity at the sample could be varied between 30 and 80 MW/cm^2 in order to irradiate the LB samples.

To avoid possible damage on the samples, caused by high intensities of strong focused beams, different neutral density filters were also implemented. The desired polarization of the fundamental beam was selected by means of an IR-coated Glan-Laser polarizer and a λ/2-Quartz-retarder. A second polarizer was used as an analyzer allowing the characterization of the SHG-light. The second harmonic wave ($\lambda_{2\omega} = 532$ nm) was detected by a sensitive photomultiplier (HAMAMATSU R-928) behind interferential optical filters centered at 532 ± 10 nm. The SHG-device was calibrated by means of a Y-cut α-quartz crystal wedged in the d_{11}-direction ($d_{11} = 0.64$ pm V^{-1}), which is frequently used as a standard NLO-reference via the *Maker-Fringes* method.

3. Results and discussion

Azobenzene is characterized spectroscopically by a low-intensity n → π* band in the visible and a high-intensity π → π* band in the UV. Substitution by an electron-donor and an electron-withdrawing group in the 4- and 4′- positions, respectively, increases the dipole moment and consequently the charge transfer (CT) character of the π → π* transition along the molecular long axis and gives rise to a red-shift of the corresponding band, which overlaps with the weak n → π* band [1]. The CT character of this band causes a strong dependence of the band position on the solvent polarity [26]. In the present work, we study the formation of CT complexes for *N*-methyl-*N*-{4-[(*E*)-(4-nitrophenyl)diazenyl] phenyl}-*N*-(3, 6, 9-trioxadecas-1-yl)amine (**RED-PEGM-3**), *N*-methyl-*N*-{4-[(*E*)-(4-nitrophenyl) diazenyl] phenyl}-*N*-(3, 6, 9, 12, 15, 18, 21, 24-octaoxapentaeicos-1-yl)amine (**RED-PEGM-8**) and *N*-methyl-*N*-{4-[(*E*)-(4-nitrophenyl) diazenyl] phenyl}-*N*-(3, 6, 9, 12, 15, 18, 21, 24, 27, 30)-decaoxauntricontas-1-yl)amine (**RED-PEGM-10**) in various environments. The structure of these dyes has been previously shown in Fig. 1.

Dipole moments of the azo-dyes were estimated by semi-empirical calculations using AM1 and PM3 methods and further by DFT calculations B3LYP/aug-cc-PVTZ(-f)//BHandH/G-31G* level of theory [25] and the results are summarized in Table 1. Both AM1 and PM3 methods predicted a higher μ value for **RED-PEGM-3** than for its homologues **RED-PEGM-8** and **RED-PEGM-10**. Longer end-capped poly (ethylene glycol) side-chains (PEGM) result in an overall decreased polarity effect on the dye. This is due to the high electron-withdrawing inductive effect, which exists along the σ bonds, due to the oxygen atoms present in the PEGM segment. Apparently, the semi-empirical PM3 method provided good correlation between the μ values obtained for the dye series. Nevertheless, the AM1 method predicted a higher μ value for **RED-PEGM-10** than for **RED-PEGM-8**. For this reason, we performed DFT calculations in order to ensure that these values were realistic. DFT methods take into account electronic correlations, which when combined with a large basis set allow one to obtain electron-density distributions in the molecule. According to this method, the polarity of the amphiphilic dyes, in decreasing order is as follows: **RED-PEGM-3** > **RED-PEGM-10** > **RED-PEGM-8**, which is quite reasonable taking into account the structure of the different azobenzenes. Methyl groups bound to the amino group contribute to enhance the inductive electron-donor effect in the molecule. That is why the results for **RED-PEGM-3** suggest that it is more polar than its homologues. All the three methods predicted lower μ values for **RED-PEGM-8** and **RED-PEGM-10**, which can be explained by the higher inductive electron-withdrawing effect of the longer PEGM chain. However, contrary to what was expected, the results suggest that **RED-PEGM-10** is more polar than **RED-PEGM-8**. This can be due to conformational arrangements of the longer PEGM segment around the azobenzene unit. Optical properties of all dyes were studied in Z-type

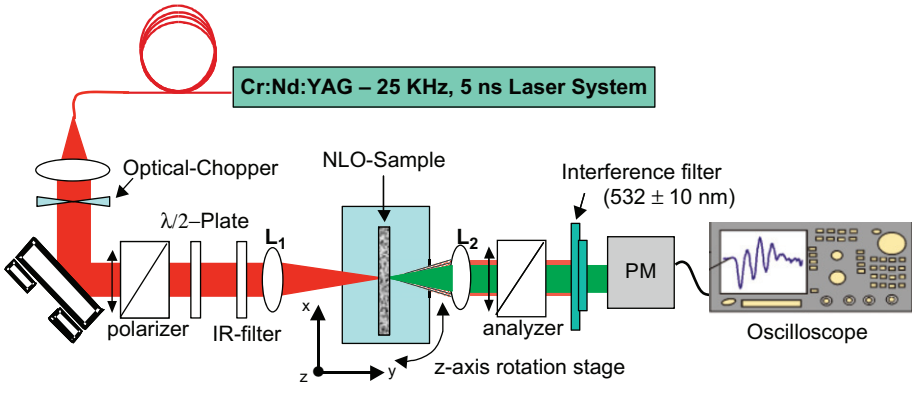

Fig. 2. Experimental set-up for SHG measurements in LB–**RED-PEGM-8** films.

Table 1
Dipole moments of the azo-dyes calculated by semi-empirical and DFT methods

Azo-dye	AM1 (D)	PM3 (D)	DFT[a] (D)
RED-PEGM-3	10.3	8.15	10.31
RED-PEGM-8	7.42	7.59	8.21
RED-PEGM-10	9.66	7.58	9.25

[a] Using B3LYP/aug-cc-PVTZ(-f)//BHandH/G-31G* method.

LB films by absorption spectroscopy and the results were compared to those previously reported in solution, cast films and Y-type LB films [24] (Table 2).

3.1. Formation of CT complexes in solution

Aggregation of **RED-PEGM** compounds was previously studied in solution, cast films and Y-type LB films by absorption spectroscopy [24]. These dyes form H-aggregates in concentrated high water content solutions and in cast films. **RED-PEGM-3** showed also to be able to form head to tail J-aggregates in cast films. ^{1}H NMR, 2D NOESY experiments confirmed that **RED-PEGM-3**, like many commercial azobenzene dyes, undergoes aggregation by parallel alignment. Also, ^{1}H NMR, 2D NOESY of **RED-PEGM-3** in CD_3OD:D_2O (20:80) at elevated concentration (Fig. 3) shows that the only interactions present are those of the aromatic protons with themselves and weak intermolecular interactions between H^1 and H^2 (spot I) (Fig. 3, see Scheme 1). Indeed, when **RED-PEGM-3** forms H-aggregates, molecules are paired in a parallel "face to face" fashion. It is very well known that this arrangement is favoured according to Davidov's theory [13]. However, **RED-PEGM-3** showed no interactions between the oligo(ethylene glycol) segment with the azobenzene unit.

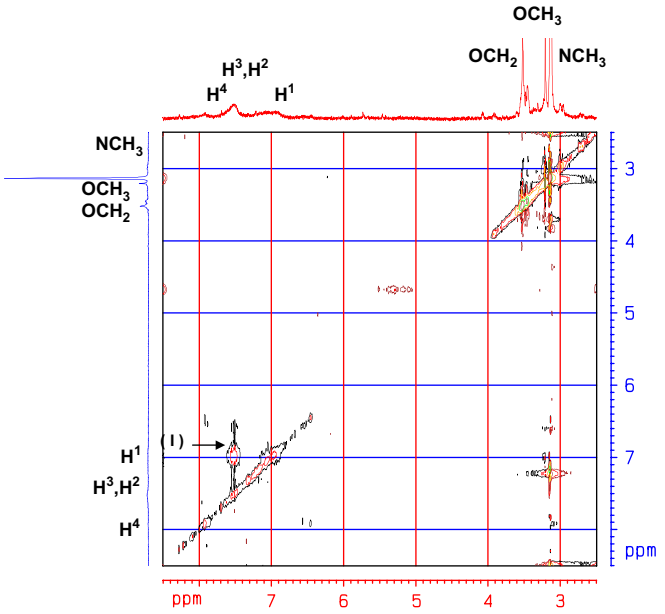

Fig. 3. ^{1}H NMR, 2D NOESY of **RED-PEGM-3** in CD_3OD:D_2O, 80:20.

^{1}H NMR, 2D NOESY data of **RED-PEGM-8** carried out in D_2O solution (Fig. 4) showed that molecules are associated in an atypical antiparallel fashion. As we can see, in the ^{1}H NMR, 2D NOESY spectrum of this dye, H^4 interacts with H^2 (spot II) and the protons of N–CH_3 interact with H^3 (spot III) and H^4 (spot IV) (Fig. 4, see Scheme 1). These interactions can only occur in an intermolecular fashion and they suggest that the molecules aggregate such that the amino group of one molecule faces the nitro group of the other. Therefore, molecules are paired in an antiparallel fashion with partial overlap of the azobenzene chromophores. This

Table 2
Absorption wavelengths for the different dyes

System	**RED-PEGM-3** (nm)	**RED-PEGM-8** (nm)	**RED-PEGM-10** (nm)
$CHCl_3$	480	477	476
THF	478	479	477
Methanol	478[a]	480[a]	479
Methanol:H_2O, 80:20	488[a]	490[a]	490
Methanol:H_2O, 60:40	492[a]	492[a]	492
Methanol:H_2O, 40:60	498[a]	498[a]	499
Methanol:H_2O, 20:80	402[a,b]	500[a]	500
	500[a]		
H_2O	–	402[a,b]	404[a]
		500[a]	500[a]
Cast film ($CHCl_3$)	407[a,b]	404[a,b]	402[b]
	490[a]	492[a]	492
	500[a,c]	508[a,c]	510[c]
Y-type LB films (40 layers)	486[a]	515[a]	–
Z-type LB films (40 layers)	478	489	–

[a] From Ref. [24].
[b] Band due to the H-aggregates.
[c] Band due to the J-aggregates.

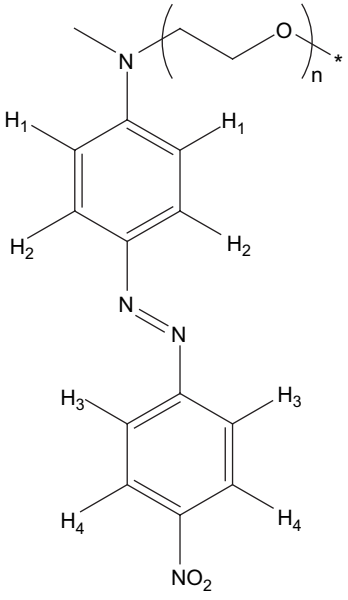

Scheme 1.

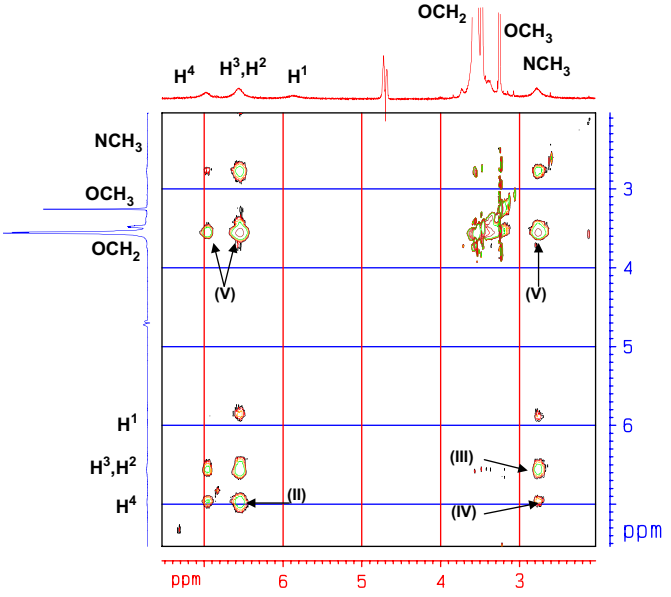

Fig. 4. ^{1}H NMR, 2D NOESY of **RED-PEGM-8** in D_2O.

can be explained by enhanced steric effects, due to the eight units of ethylene glycol in the PEGM segment making the molecule rather bulky. A similar behaviour was reported for azo-polymers of the pXMAN series in spin-cast films [27,28]. Antiparallel association is uncommon for the majority of aromatic compounds according to Davidov's theory [13]. **RED-PEGM-10** behaved similarly and ^{1}H NMR, 2D NOESY of this dye in D_2O solution is shown in Fig. 5.

Another interesting fact is that both ^{1}H NMR, 2D NOESY spectra of **RED-PEGM-8** and **RED-PEGM-10** show significant interaction of the OCH_2 protons of the PEGM chain with protons H^2, H^3 and H^4 and $N{-}CH_3$ (spots V) (Figs. 4 and 5, see Scheme 1). This shows the evidence of the formation of an intramolecular CT complex in aqueous solutions due to the coiling of the long PEGM segment around the azobenzene unit. In **RED-PEGM-8**, the poly(ethylene glycol) segment is long enough to surround the aromatic group, thereby stabilizing the electron-withdrawing nitro group with the electron rich oxygen atoms of the PEGM chain. In addition, the hydrophilic PEGM segment likely protects the hydrophobic azobenzene group from the aqueous medium. In addition, ^{1}H NMR, 2D NOESY spectra of **RED-PEGM-10** (Fig. 5, see Scheme 1) revealed also the formation of atypical H-aggregates. As we can see, the protons of $N{-}CH_3$ interact with H^4 and H^3 (spots VI); H^1 interacts with H^3 and H^4 (spots VII); H^4 showed strong interactions with H^3 (spot VIII). Such kinds of interactions can only occur in an intermolecular fashion when the azobenzene molecules are paired antiparallel.

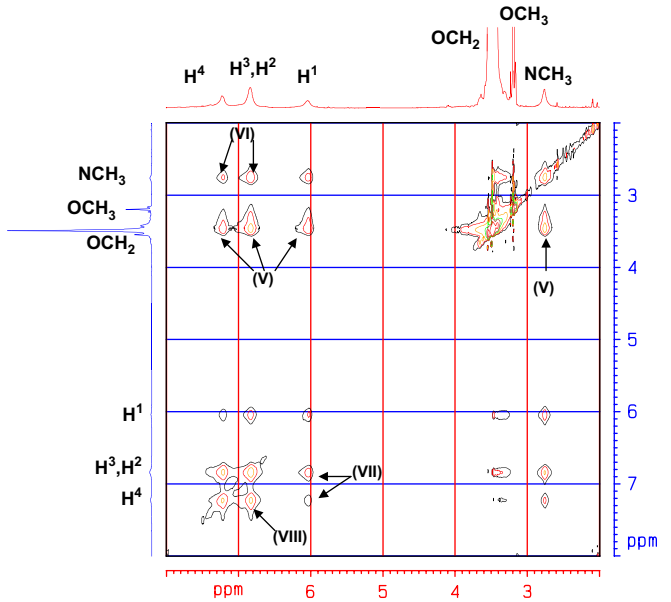

Fig. 5. ^{1}H NMR, 2D NOESY of **RED-PEGM-10** in D_2O.

A conformational analysis of the different **RED-PEGM** molecules estimated by DFT calculations taking into account the polarity of the solvent, provided the most stable conformer for each of these dyes in solution in the non-associated state, as illustrated in Fig. 6. Unlike **RED-PEGM-8** and **RED-PEGM-10**, the shorter PEGM chain of **RED-PEGM-3** is not able to surround the aromatic part of the molecule to form such kinds of complexes. In the lowest energy conformer of **RED-PEGM-3** ($E = -1355.726889$ a.u.) (Fig. 6A), the PEGM chain slightly coils around the amino substituted phenyl

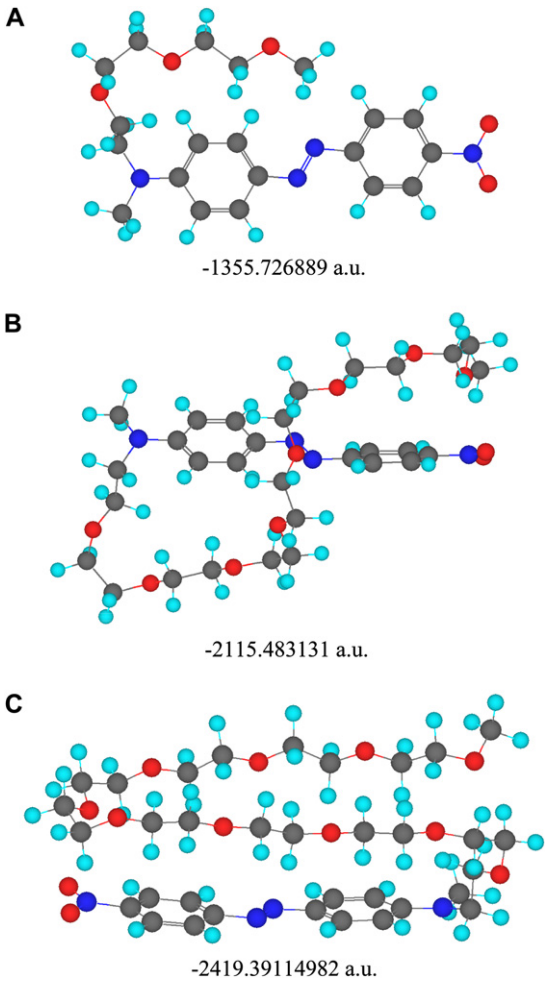

Fig. 6. Conformational analysis for the different **RED-PEGM** dyes obtained by DFT calculations.

group showing only a slight interaction between the protons H^2 (see Scheme 1) and the protons present in the methylene groups of the PEGM. In this case the PEGM chain is not long enough to interact with H^3 and H^4. By contrast, in the more stable geometry of **RED-PEGM-8** ($E = -2115.483131$ a.u.) (Fig. 6B), the longer PEGM chain coils around the aromatic unit passing below and above the azobenzene plane, thus favouring significant interactions between the aromatic protons H^2, H^3 and H^4 (see Scheme 1) with the protons of the PEGM segment. Finally, in the most stable conformer of **RED-PEGM-10** ($E = -2419.39114982$ a.u.) (Fig. 6C) the long PEGM chain coils around the aromatic unit, passing above the azobenzene plane. This gives rise to strong intramolecular interactions between the protons present in the PEGM segment and those present in the aromatic portion of the molecule. The geometries predicted by molecular modelling shown in Fig. 6 agree well with the results obtained by ^{1}H NMR, 2D NOESY spectroscopy.

3.2. Preparation of Langmuir–Blodgett films

We prepared Z-type LB films of the different **RED-PEGM** dyes using quartz and glass as substrates. **RED-PEGM-3** was not shown to be amphiphilic enough to get good quality regular multilayer LB films. On the other hand, it was quite difficult to get suitable LB films of **RED-PEGM-10** because of its low melting point (30 °C). Thus, **RED-PEGM-8** was the best option for the generation of built up multilayer systems and therefore, Z-type LB films were prepared with this dye.

Fig. 7 shows the surface pressure–area isotherm of the **RED-PEGM** dyes during the compression process, reaching the solid phase at a molecular area about 26 Å^2. For **RED-PEGM-8**, the monolayer exhibited a high collapse pressure of about 50 mN/m, and the large liquid-condensed region indicates that stable condensed films are formed on water. Reversible compression isotherms of the surface pressure–area at a pressure of 20 mN/m were observed for a monolayer of this dye suggesting that an irreversible rearrangement does not occur upon cycling. Moreover, BAM images monitoring the formation of Langmuir films of **RED-PEGM-8** are shown in Fig. 8. As we can see, a high quality homogeneous film is formed during compression (from 33 to 24 Å^2) (Fig. 8A–D), however, the film does start to collapse by the end of the compression process (Fig. 8e).

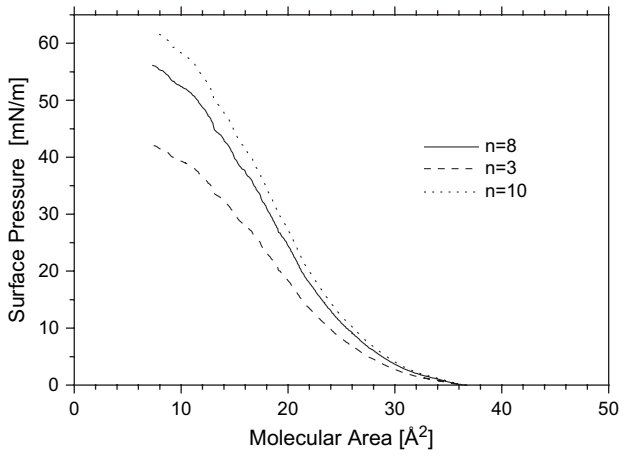

Fig. 7. Surface pressure–area isotherms of **RED-PEGM** dyes.

Fig. 9 shows the AFM images of the Z-type bilayer films of **RED-PEGM-8**, where the film presents full surface coverage and regioregular texture. Absorption spectra of **RED-PEGM-8** Z-type LB films are shown as a function of the number of layers in Fig. 10. The absorption increases linearly with the number of layers, which indicates that deposition takes place regularly for up to 40 layers of Z-type deposition.

Z-type LB films of **RED-PEGM-8** (Fig. 10) exhibit a maximum absorption wavelength at $\lambda = 489$ nm after 40 layers, which is red-shifted when compared to the monolayer ($\lambda = 472$ nm). Apparently no J-aggregation is present, however, the results suggest that H-aggregation is present since the monolayer LB film exhibits a blue shifted absorption band as compared to the 40-layer absorption.

3.3. SHG measurements

The LB-deposition technique has been commonly implemented as a practical alternative to poled spin-coated organic films in order to create oriented molecular systems of push–pull NLO-chromophores due to the non-centrosymmetric structure presented by the Z-type LB mono- and multilayer systems, as required for second order NLO-effects [29–31]. According to the original experimental studies concerning to SHG of LB-structures [32,33], the investigated Z-type LB **RED-PEGM-8** samples exhibit a quadratic relation between the observed SH-intensity and the number of layers deposited on the glass substrate.

As shown in Fig. 11, a linear dependence between the square root of the SH-signal and the number of deposited Z-type LB-layers can be observed (layers number were varied in steps of 10, from 1 to 40, as expected no SHG was observed for clean glass substrates). The linear relationship may deviate with an increased number of deposited layers since the last point (for $N = 40$) slightly drops from the linear fit, suggesting that the system becomes more unstable as the number of layers increases. The SH-intensity generated by these samples has been measured at an incidence angle of 45° with an S–P and P–P polarization geometries because at this angle, maximal fundamental excitation can be achieved in order to produce highest SH-signal in rod-like molecules.

For comparison purposes, the calibrated SH-signal of a Y-cut α-quartz crystal was compared with the SHG-response of an LB-layer and according to the *Maker-Fringes* method (by angle dependent SHG measurements, not shown here), a major contribution of the $\chi^{(2)}_{31}$ and $\chi^{(2)}_{33}$ NLO-tensor coefficients of the studied molecules was observed. For a non-normal incident laser beam polarized parallel to the plane of incidence, the $\chi^{(2)}_{31}$ and $\chi^{(2)}_{33}$-components of an LB-layer sample were evaluated to approximately 2.7 and 12.5 pm V^{-1} respectively.

Since the SH-signal produced by this kind of system shows a functional dependence with the sample thickness, a better NLO-response is observed for thicker films, where the $\chi^{(2)}_{31}$

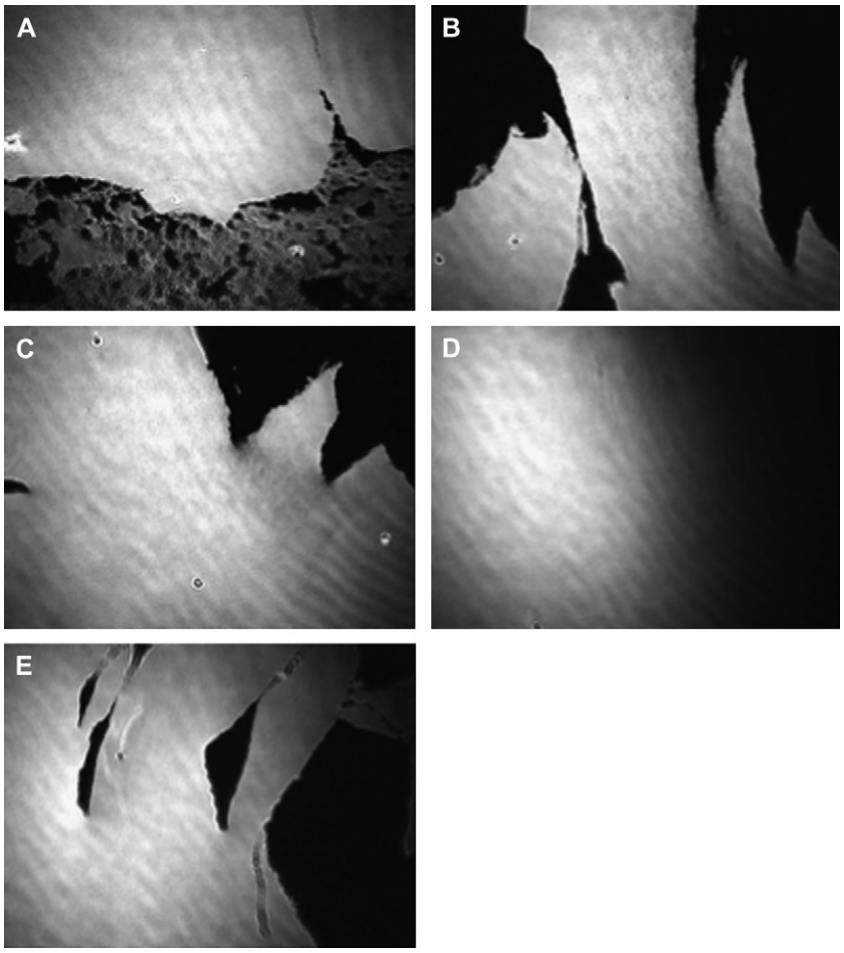

Fig. 8. BAM images for **RED-PEGM-8** at (A) $A = 33$ Å^2, (B) $A = 28$ Å^2, (C) $A = 26$ Å^2, (D) $A = 24$ Å^2, and (E) during decompression (collapse).

and $\chi^{(2)}_{33}$-coefficients increase roughly with $N\chi^{(2)}_{ij}(i = 3,\ j = 1, 3)$, respectively, N being, the number of monolayers [34]. Present studies concerning the aggregation conditions and the optimization of the molecular concentration within the precursor solvent–chromophore system are currently under way in order to improve the NLO-response of the deposited LB-layers. However, the wide absorption band centered in the visible region for the LB **RED-PEGM-8** samples will

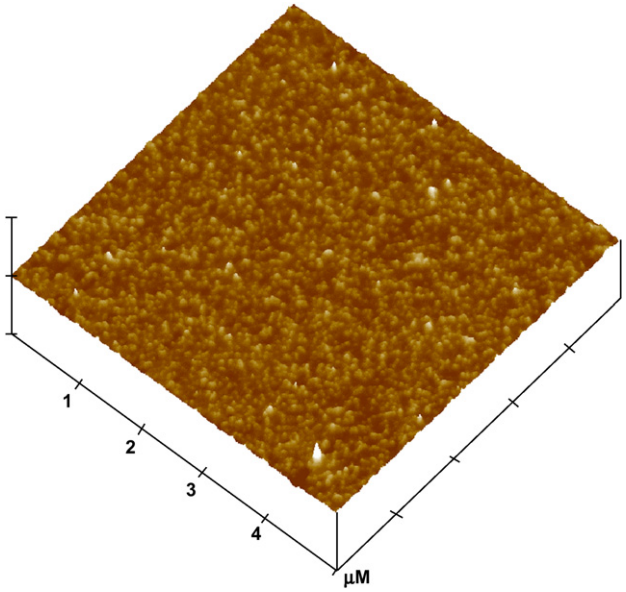

Fig. 9. AFM images of a Z-type LB film of **RED-PEGM-8**.

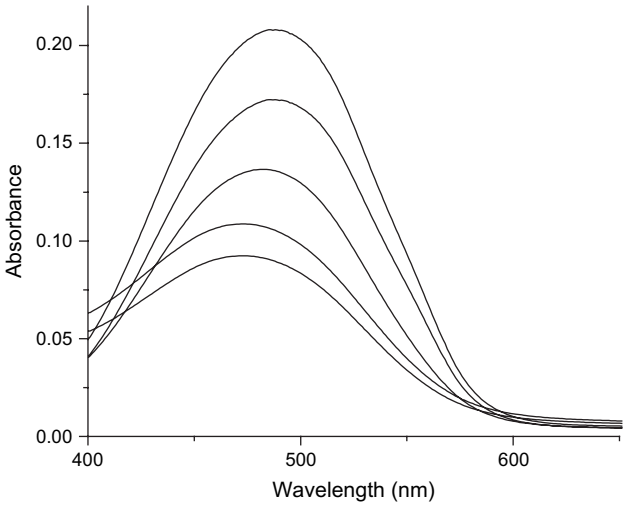

Fig. 10. Absorption spectra of the Z-type LB films of **RED-PEGM-8** (from bottom to top: 2, 10, 20, 30, and 40 layers).

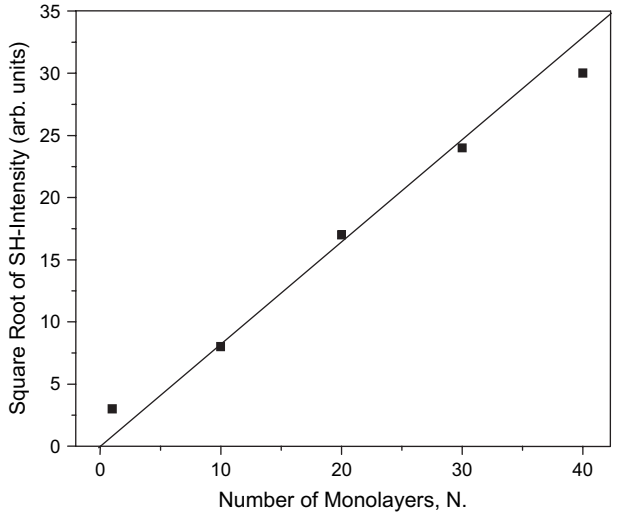

Fig. 11. Linear dependence observed at room temperature, between the square root of the SH-intensity of different **RED-PEGM-8** LB-multilayer systems and the number of deposited layers, *N*.

produce a moderate SHG-response of these systems by working with the standard fundamental wave of a YAG laser system, where the SHG-response is highly absorbed still when the dipolar moment of this compound is relatively high. Further investigations of the quadratic non-linear optical response of the LB **RED-PEGM-8** samples as a function of the irradiation wavelength, implementing an Optical Parametric Oscillator (OPO)-Laser system will be necessary in order to identify better condition for SHG applications.

4. Conclusion

^{1}H NMR, and 2D NOESY experiments revealed that **RED-PEGM-8** and **RED-PEGM-10** form atypical antiparallel H-aggregates in aqueous solution, jointly with the formation of intramolecular CT complexes by the coiling of the PEGM chain around the azobenzene unit. Z-type LB films of **RED-PEGM-8** showed measurable SHG-activity, the $\chi^{(2)}_{31}$ and $\chi^{(2)}_{33}$ NLO-tensor coefficients were evaluated for a single monolayer to be 2.7 and 12.5 pm V^{-1} respectively, from which an order parameter of $S = 0.31$ can be evaluated. This last finding indicates a tilted molecular organization within the LB-layers which should be improved in order to achieve higher $\chi^{(2)}$-effects in a perpendicular-close molecular arrangement. In principle, this could be done by varying the conditions such as the targeted surface pressure–area and the substrate dipper speed that is used to obtain the monolayers, which will be done in future works.

Acknowledgements

We are grateful to DGAPA-UNAM (PAPIIT IN112203 and IN102905) for financial support. We also thank Miguel Angel Canseco for his help with absorption spectra and Dr. Margarita Rivera for her assistance with AFM images.

References

[1] Jonsson B, Lindman B, Homberg K, Kronberg B. Surfactants and polymers in aqueous solution. Chichester: John Wiley & Sons; 1998. p. 91.
[2] Skotheim TA, Elsenbaumer RL, Reynolds JF. Handbook of conducting polymers. 2nd ed. New York: Marcel Dekker; 1998.
[3] Foster R. Organic charge transfer complexes. London: Academic Press; 1969. p. 4.
[4] Cojocariu G, Natansohn A. Macromolecules 2001;79:3827–9.
[5] Rau H. In: Rabek JK, editor. Photochemistry and photophysics, vol. 2. Boca Raton, FL: CRC Press; 1990. p. 119.
[6] Natansohn, Rochon P. Can J Chem 2001;7:1093–100.
[7] Todorov T, Nikalova L, Tomova N. Appl Opt 1984;23:4309.
[8] Xie S, Natansohn A, Rochon P. Chem Mater 1993;5:403–11.
[9] Viswanathan NK, Kim DY, Bian S, Williams J, Liu W, Li L, et al. J Mater Chem 1999;9:1941.
[10] Ichimura K. Chem Rev 2000;100:1847–74.
[11] Delaire JA, Nakatani K. Chem Rev 2000;100:1817–46.
[12] Natansohn A, Rochon P. Chem Rev 2002;102:4139–75.
[13] Kasha M. Radiat Res 1963;20:55–71.
[14] He XH, Zhang HL, Yan DL, Wang X. J Polym Sci Part A Polym Chem 2003;41:2854–64.
[15] Tian YQ, Watanabe K, Kong XX, Abe J, Iyoda T. Macromolecules 2003;36:39–47.
[16] Saito M, Shimomura T, Okumura Y, Ito K, Hayakawa R. J Chem Phys 2001;114:1–3.
[17] Shimomura T, Funaki T, Ito K. J Inclusion Phenom Macrocycl Chem 2002;44:275–8.
[18] Zheng PJ, Wang C, Hu X, Tam KC, Li L. Macromolecules 2005;38:2859–64.
[19] Hu X, Zheng PJ, Zhao XY, Li L, Tam KC, Gan LH. Polymer 2004;45:6219–25.
[20] Takashima Y, Nakayama T, Miyauchi M, Kawaguchi Y. Chem Lett 2004;33:890–1.
[21] Ikeda T, Ooya T, Yui N. Polym J 1999;31:658–63.
[22] Tung CH, Wu LZ, Zhang LP, Chen B. Acc Chem Res 2003;36: 39–47.
[23] Rivera E, Belletête M, Natansohn A, Durocher. Can J Chem 2003;81:1076–82.
[24] Rivera E, Carreón-Castro MP, Buendía I, Cedillo G. Dyes Pigments 2006;68:217–26.
[25] Dewar MJW, Dieter K. J Am Chem Soc 1986;108:8075.
[26] Shin DM, Schanze KS, Whitten DG. J Am Chem Soc 1989;111:8494–501.
[27] Freiberg S, Lagugné-Labarthet F, Rochon P, Natansohn A. Macromolecules 2003;36:2680–8.
[28] Iftime G, Lagugné-Labarthet F, Natansohn A, Rochon P. J Am Chem Soc 2000;122:12646.
[29] Nalwa HS, Miyata S. Non-linear optics of organic molecules. CRS Press Inc.; 1997.
[30] Roberts G. Langmuir–Blodgett films. Plenum Press; 1990.
[31] Kajzar F, Swalen JD. Organic thin films for waveguiding non-linear optics. Gordon and Breach Publishers; 1996.
[32] Davis SG, Polywka MEC, Richardson T, Roberts GG. Br. Patent 8717566; 1988.
[33] Decher G, Tieke B, Bosshard G, Gunter P. Ferroelectrics 1989; 91:193.
[34] Prasad PN, Williams DJ. Introduction to non-linear optical effects in molecules and polymers. John Wiley & Sons, Inc.; 1991. p. 17.